12-2010

Late Quaternary slip rate on the Kern Canyon fault at Soda Spring, Tulare County, California

Colin B. Amos
Western Washington University, colin.amos@wwu.edu

Keith I. Kelson

Dylan H. Rood

David T. Simpson

Ronn S. Rose

Late Quaternary slip rate on the Kern Canyon fault at Soda Spring, Tulare County, California

Colin B. Amos[1,*], Keith I. Kelson[1], Dylan H. Rood[2,3], David T. Simpson[4], and Ronn S. Rose[5]
[1]WILLIAM LETTIS & ASSOCIATES, INC., WALNUT CREEK, CALIFORNIA 94596, USA
[2]CENTER FOR ACCELERATOR MASS SPECTROMETRY, LAWRENCE LIVERMORE NATIONAL LABORATORY, LIVERMORE, CALIFORNIA 94550, USA
[3]DEPARTMENT OF EARTH SCIENCE, UNIVERSITY OF CALIFORNIA, SANTA BARBARA, CALIFORNIA 93106, USA
[4]URS CORPORATION, 1333 BROADWAY, SUITE 800, OAKLAND, CALIFORNIA 94612, USA
[5]DAM SAFETY ASSURANCE PROGRAM, U.S. ARMY CORPS OF ENGINEERS, SACRAMENTO, CALIFORNIA 95814, USA

ABSTRACT

The Kern Canyon fault represents a major tectonic and physiographic boundary in the southern Sierra Nevada of east-central California. Previous investigations of the Kern Canyon fault underscore its importance as a Late Cretaceous and Neogene shear zone in the tectonic development of the southern Sierra Nevada. Study of the late Quaternary history of activity, however, has been confounded by the remote nature of the Kern Canyon fault and deep along-strike exhumation within the northern Kern River drainage, driven by focused fluvial and glacial erosion. Recent acquisition of airborne lidar (light detection and ranging) topography along the ~140 km length of the Kern Canyon fault provides a comprehensive view of the active surface trace. High-resolution, lidar-derived digital elevation models (DEMs) for the northern Kern Canyon fault enable identification of previously unrecognized offsets of late Quaternary moraines near Soda Spring (36.345°N, 118.408°W). Predominately north-striking fault scarps developed on the Soda Spring moraines display west-side-up displacement and lack a significant sense of strike-slip separation, consistent with detailed mapping and trenching along the entire Kern Canyon fault. Scarp-normal topographic profiling derived from the lidar DEMs suggests normal displacement of at least 2.8 +0.6/–0.5 m of the Tioga terminal moraine crest. Cosmogenic ^{10}Be exposure dating of Tioga moraine boulders yields a tight age cluster centered around 18.1 ± 0.5 ka (n = 6), indicating a minimum normal-sense fault slip rate of ~0.1–0.2 mm/yr over this period. Taken together, these results provide the first clear documentation of late Quaternary activity on the Kern Canyon fault and highlight its role in accommodating internal deformation of the southern Sierra Nevada.

LITHOSPHERE; v. 2; no. 6; p. 411–417; Data Repository 2010266. doi: 10.1130/L100.1

INTRODUCTION

The significance of the Kern Canyon fault as a first-order geologic structure within the southern Sierra Nevada has been recognized for over a century (Lawson, 1904; Webb, 1946; Ross, 1986). More recent work has focused on the role of the Kern Canyon fault in accommodating Late Cretaceous ductile deformation within the Sierra Nevada arc (e.g., Busby-Spera and Saleeby, 1990; Nadin and Saleeby, 2008) and later brittle remobilization of the Kern Canyon fault in the Neogene (Nadin and Saleeby, 2008; Saleeby et al., 2009). Quaternary activity, however, was precluded by the seminal work of Webb (1946), who reported the presence of an undeformed basalt-capped terrace, later dated at 3.5 Ma using K-Ar techniques (Dalrymple, 1963), overlying the Kern Canyon fault. Renewed interest in the activity of the Kern Canyon fault, related to its presence beneath the Lake Isabella Auxiliary Dam (Fig. 1) challenges Webb's original interpretation and demonstrates clear displacement of this basalt flow (Page, 2005, personal commun.), confirming the Kern Canyon fault as a primary seismogenic source in the southern Sierra Nevada. Because of the importance of the Kern Canyon fault to nearby engineered facilities, a detailed and comprehensive assessment of the fault characteristics has been conducted to determine the rate, timing, and sense of Quaternary displacement on the Kern Canyon fault (Kelson et al., 2010).

As part of the seismic safety study of the Lake Isabella dams, the U.S. Army Corps of Engineers commissioned an airborne lidar survey to collect high-resolution topographic data spanning the entire ~140 km length of the Kern Canyon fault. These data were used to aid paleoseismic investigations along the fault, to be summarized in a later paper, and to identify and characterize displaced late Quaternary geomorphic surfaces and/or sediments within the remote, rugged terrain of northern Kern Canyon. Despite well-preserved bedrock scarps along much of the Kern Canyon fault (Ross, 1986; Saleeby et al., 2009), vigorous erosion within the Kern Canyon and a general lack of sufficiently old deposits to record faulting have hindered efforts to locate reliable Quaternary offsets. In this paper, we describe a site along the northern Kern Canyon fault (Soda Spring, Fig. 1), where displaced glacial moraines provide definitive evidence for late Pleistocene movement along the Kern Canyon fault. These landforms serve as ideal geomorphic piercing lines to reconstruct and quantify fault displacement using the lidar topography. Detailed geomorphic mapping and analysis of the lidar data reveal a clear and consistent sense of normal offset for each of three generations of nested terminal moraines at the Soda Springs site. Cosmogenic ^{10}Be dating of moraine boulders on the youngest of these landforms yields an estimate of the fault slip rate over the late Quaternary.

*Current address: Department of Earth and Planetary Science, University of California, Berkeley, California 94720, USA.

Editor's note: This article is part of a special issue devoted to the GSA Field Forum titled Structure and Neotectonic Evolution of Northern Owens Valley and the Volcanic Tableland, California, convened by David A. Ferrill, Southwest Research Institute, Alan P. Morris, Southwest Research Institute, and Nancye H. Dawers, Tulane University. More papers on this subject will follow in subsequent issues, and these will be collected online at http://lithosphere.gsapubs.org/ (click on Themed Issues).

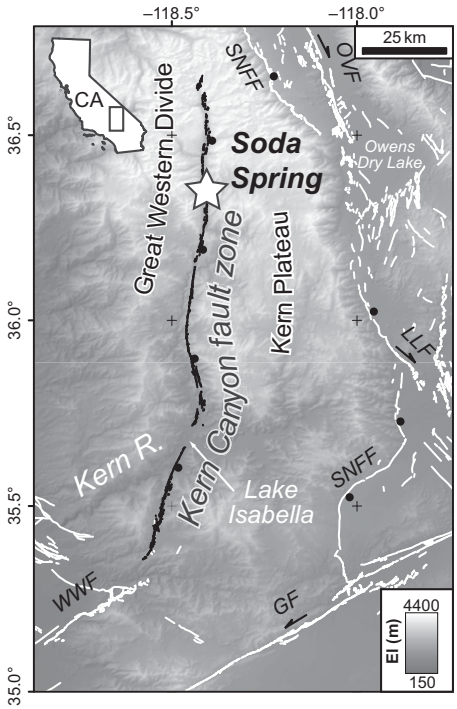

Figure 1. Overview map of the Kern Canyon fault zone showing the surface trace mapped from lidar data. Other major Quaternary active faults in the southeastern Sierra Nevada region are abbreviated as follows: GF—Garlock fault; LLF—Little Lake fault; OVF—Owens Valley fault; SNFF—Sierra Nevada frontal fault; WWF—White Wolf fault. Arrows indicate the slip sense of predominately strike-slip faults, while the black ball shows the downthrown side of predominately normal faults.

Considered in the larger tectonic framework of the region, our results suggest that the Kern Canyon fault contributes to regional deformation patterns in the southern Sierra Nevada.

STUDY AREA

The northern Kern River canyon represents a remarkable physiographic and geomorphic feature bisecting the southern Sierra Nevada and separating the Great Western Divide from the Kern Plateau to the east (Fig. 1). Soda Spring is situated at the floor of the northern Kern River canyon at an elevation of ~2000 m, near the confluences of Coyote and Golden Trout Creeks (Fig. 2). This location marks the geomorphic boundary between the relatively broad, U-shaped glacial valley of the northern Kern River canyon and the comparatively narrow gorge to the south. North of Soda Spring, the U-shaped Kern River canyon is inset within a series of relict, low-relief upland erosion surfaces below the surrounding peaks of the high southern Sierra Nevada (Lawson, 1904; Matthes, 1937; Webb, 1946; Clark et al., 2005) (e.g., the Chagoopa Plateau; Fig. 3A). Total relief between these surfaces and the river below is ~500–600 m in the vicinity of Soda Spring.

Detailed mapping of glacial deposits and landforms at Soda Spring was completed using color orthophotos and hillshade images derived from the lidar topography (Fig. 2). This mapping reveals three generations of nested terminal and recessional moraines and associated outwash surfaces, as well as extensive late Pleistocene alluvial fans, fluvial terraces, and colluvial deposits (Fig. 2). Moraine loops at Soda Spring consist of unsorted glacial till derived primarily from felsic plutonic rocks in the upper Kern River headwaters. Relatively younger moraines are inset within older moraine loops, resulting in a south-to-north age progression from oldest to youngest (Fig. 2). Geomorphic characteristics of these moraines vary according to their relative age, and the degree of erosional reworking, modification, channelization, and moraine crest diffusion increases for relatively older moraine loops. Qualitatively, the surface frequency of large boulders up to several meters in diameter also varies according to this pattern, with significantly rockier moraine crests associated with the younger moraines. Inset recessional moraine loops are present within the two oldest moraine sets at Soda Spring. Erosion by the Kern River has removed recessional moraines from the youngest, northernmost loop (Fig. 2).

Glacial features at Soda Spring were first identified by Lawson (1904) and later described by Matthes (1960), who correlated them with the Wisconsin, or Last Glacial period. The relative size, geomorphic character, and position of these features within the landscape support correlation of the Soda Spring moraines with the Tioga, Tahoe, and pre-Tahoe glaciations (Fig. 2), using the existing nomenclature of glacial subdivisions in the Sierra Nevada (e.g., Gillespie and Zehfuss, 2004).

QUANTIFYING FAULT OFFSET FROM LIDAR DATA

Lidar data spanning the length of the Kern Canyon fault was collected and processed by Towill, Inc., to provide a comprehensive topographic model along the surface trace of the fault. The lidar data set encompasses the entire ~140 km length of the Kern Canyon fault in a swath 1–5 km wide. Airborne surveying of the Soda Spring site was completed in July 2008. Bare-earth topography was constructed from the raw laser returns by filtering out nonground returns using methods proprietary to the vendor. The spatial density of ground returns varies throughout the data set and is generally greatest in areas of swath overlap and for terrain characterized by sparse vegetation and relatively low topographic relief. The ground return density for the data tiles encompassing the rugged and forested Soda Spring site averages 3.24 returns m^{-2}. Regularized grids were created from the ground returns using natural neighbor interpolation in the 3D Analyst extension of ArcGIS. A grid spacing of 0.61 m (2 ft) was chosen for the resultant DEMs to optimize data accuracy and file size. The accuracy of the bare-earth model grids was assessed through comparison with stereo photogrammetry performed in conjunction with the lidar surveying tied to surveyed ground control points and airborne Global Positioning System (GPS). The stated root mean square errors for the vertical and horizontal accuracy of the model grids are <15 cm and <30 cm, respectively.

At Soda Spring, hillshade images computed from the bare-earth lidar topography reveal roughly north-south–striking scarps along the Kern Canyon fault directly west of the Kern River (Figs. 2A, 3B, and 3C). In the southern part of the map area, the fault abuts a linear bedrock ridge impounding the southern half of the Coyote Creek fan (Fig. 2). Northward, younger fan materials bury the Kern Canyon fault trace except along an older, isolated fan remnant adjacent to Soda Spring. Where it intersects the Tahoe moraine loop, the fault trace has an average strike of ~N10°E before branching into two subparallel, north-striking splays crossing the Tioga moraine (Fig. 2). These fault strands are relatively subtle in the aerial photos and when viewed using the first-return lidar data. The bare-earth hillshade image (Figs. 3B and 3C), however, reveals both strands as prominent lineaments forming ~3–5-m-high, east-facing scarps where they intersect the Tioga moraine. The westernmost of these splays juxtaposes an isolated bedrock knob against moraine material, while the eastern strand displaces the moraine crest before disappearing beneath active Kern River alluvium to the north (Figs. 2 and 3C). Continuity of both the Tahoe and Tioga moraine loops across the fault (Fig. 2B) also suggests that slip on the northern Kern Canyon fault is predominantly normal, with little or no lateral component of displacement. Overall, the relatively straight map pattern of the fault trace at Soda Spring and its intersection with the rugged topography north of Lake Isabella suggests a steep eastward dip for the Kern Canyon fault in the shallow subsurface (Fig. 2).

The lidar topography provides a means to quantify fault displacement from the offset Soda Spring moraine crests. We follow the methodology outlined by Thompson et al. (2002) for calculating vertical separation, fault slip, slip

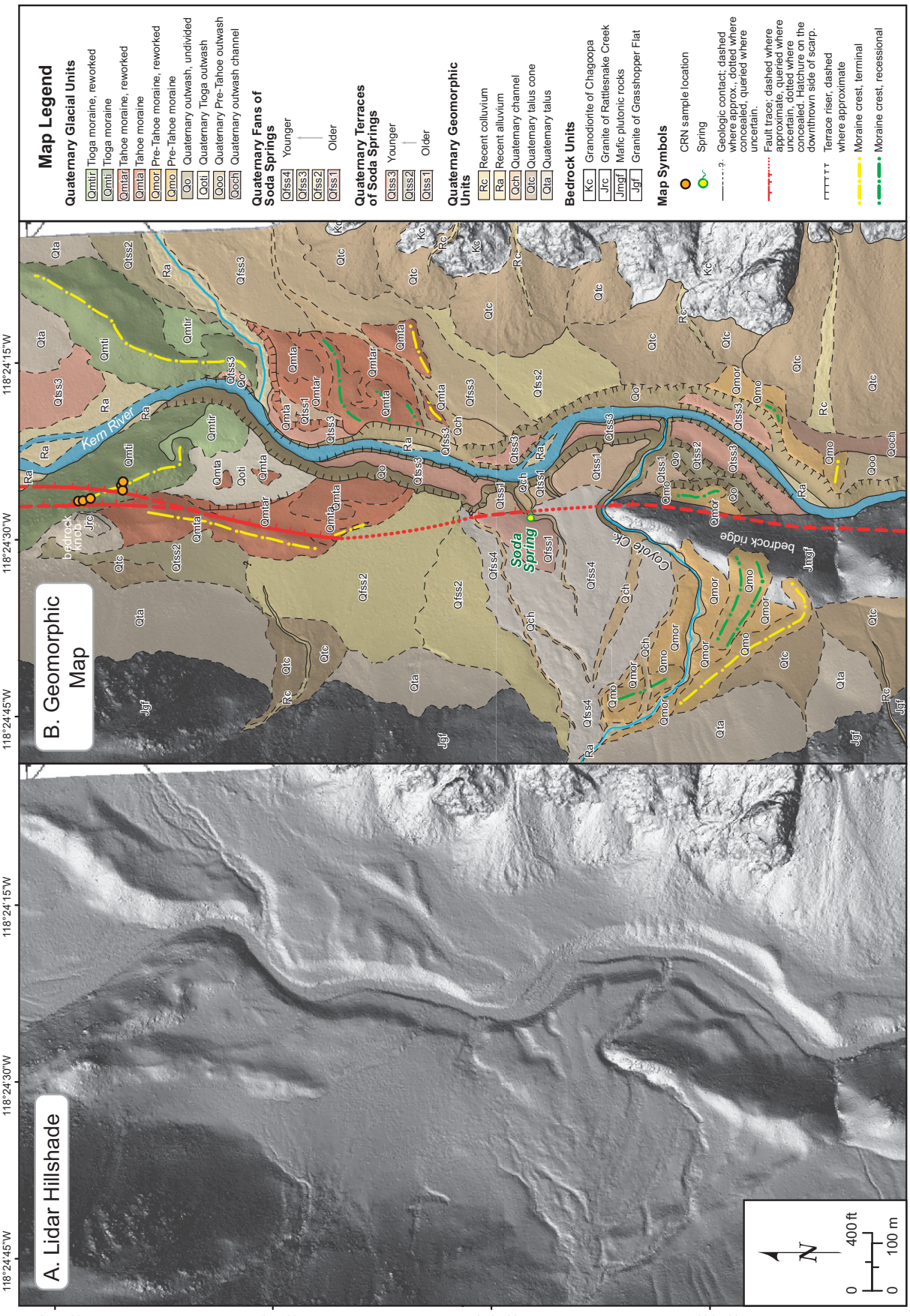

Figure 2. (A) Bare-earth hillshade image from lidar data and (B) the results of geologic and geomorphic mapping of the northern Kern Canyon fault at Soda Spring. Bedrock units are reported by Moore and Sisson (1984). CRN—cosmogenic radionuclide.

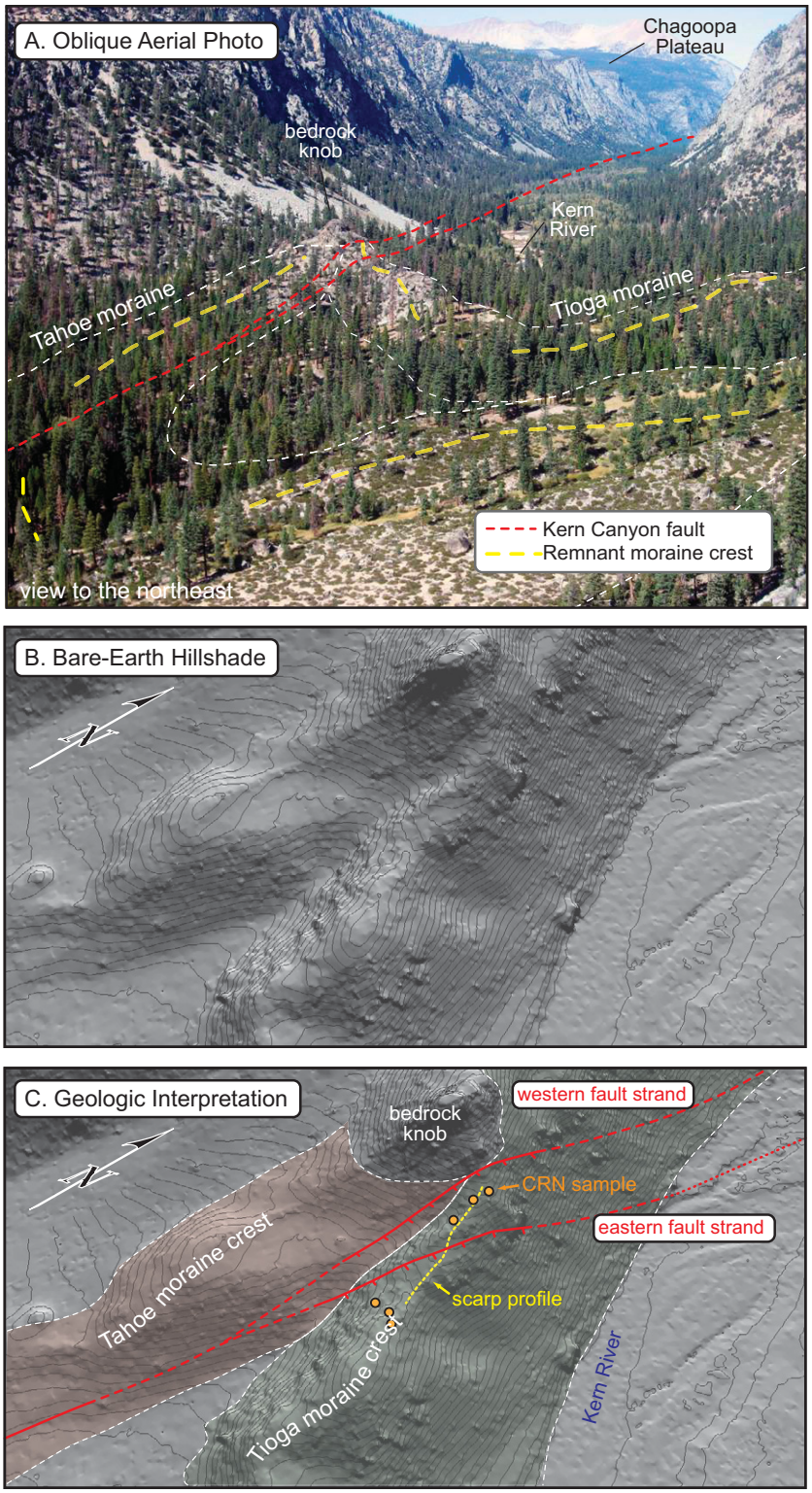

Figure 3. (A) Oblique aerial image of the Soda Spring site near the intersection of the northern Kern Canyon fault with the Tioga and Tahoe moraines. The fault trace continues northward from Soda Spring along the floor of the U-shaped northern Kern Canyon. Total relief between the Chagoopa Plateau and the Kern River Canyon floor is approximately 500–600 m near Soda Spring. (B–C) Oblique perspective view of the offset Tioga moraine crest from bare-earth lidar hillshade images. Scale varies in this perspective, but the scarp profile in C is ~90 m long; 5 ft elevation contours are also shown in each image. CRN—cosmogenic radionuclide.

rate, and the associated uncertainties from topographic profiles extracted from the bare-earth topography. These calculations depend on linear regressions through the moraine crests on both sides of the fault, as well as through the scarp face (Fig. 4), in addition to estimates of fault dip and position and the age of the offset moraine. Monte Carlo simulations sample probability distributions associated with these input variables to generate the most likely value of vertical separation, fault displacement, fault slip rate, and the associated 95% confidence intervals (Thompson et al., 2002). The Monte Carlo approach presents the distinct advantage of enabling parameterization of each input variable in our calculations as an individual probability distribution. In this routine, standard errors calculated for regression slopes and intercepts along the topographic profiles are modeled as normally distributed. Because the fault plane is nowhere exposed at Soda Spring, we rely on observations of fault dip from trenching elsewhere along the Kern Canyon fault and the intersection of the fault with topography to qualitatively constrain the fault as steeply east-dipping. We modeled the fault geometry in the Monte Carlo simulation accordingly, using a uniform distribution assigning equal likelihood to fault dips between 60° and 90°. Fault displacement also depends on the location of intersection between the fault plane and the scarp face (Fig. 4). As such, we used a trapezoidal distribution of fault positions maximized between one third and one half of the total scarp height to approximate observations of fault position for other studied normal faults (McCalpin, 1987).

Reported values of vertical separation, fault displacement, and slip rate reflect the modes and 95% confidence intervals of histograms resulting from 100,000 trial outputs from the Monte Carlo simulation.

The Tioga moraine crest provides the best piercing line across the Kern Canyon fault at Soda Spring. An abundance of large boulders and the consistency of geomorphic slopes directly adjacent to the fault (Fig. 4A) indicate that this part of the moraine crest is relatively intact and unaffected by erosion or reworking. Topographic profiling across the eastern fault strand where it intersects the moraine crest suggests 2.6 ± 0.4 m of vertical separation, corresponding to 2.8 +0.6/–0.5 m of normal fault slip given a range of dips from 60° to 90° (Fig. 4A). Given the lack of intact moraine crests preserved across the adjacent western fault strand, this value represents a minimum estimate of total fault displacement. The approximately accordant height of Tioga moraine material on either side of the western fault strand (Fig. 3C) indicates that the

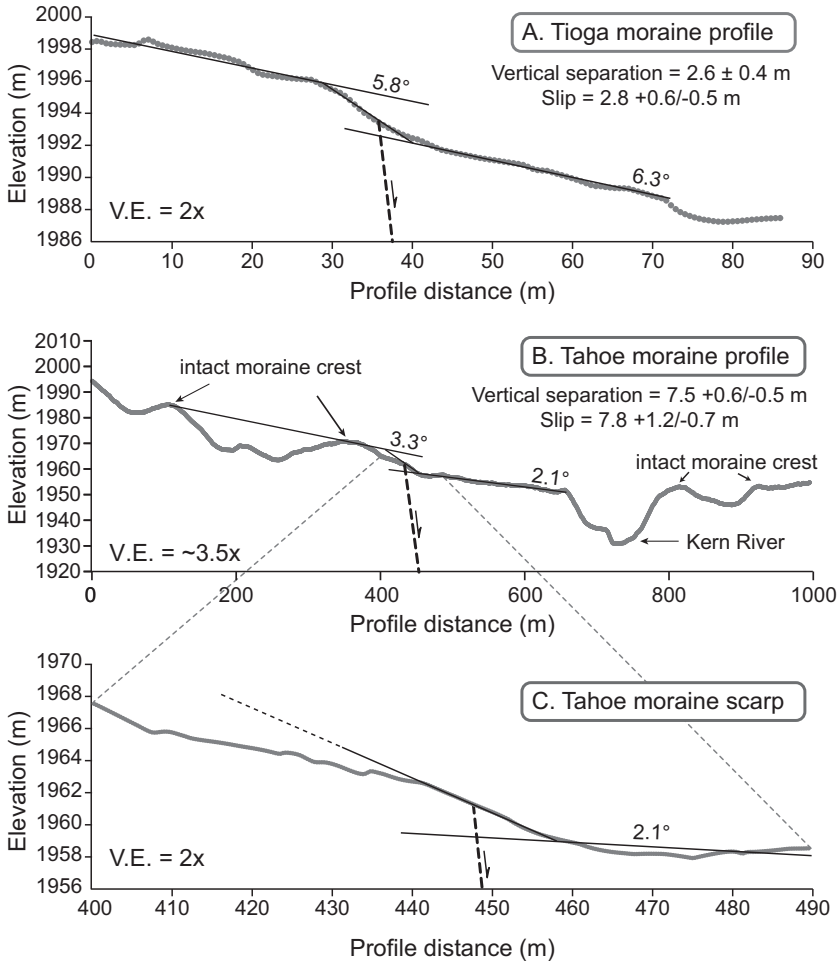

Figure 4. Topographic profiles extracted from the lidar topography showing regressions through intact portions of the (A) Tioga and (B) Tahoe moraine crests used in estimating vertical separation and displacement of these features across the Kern Canyon fault. (C) A topographic scarp, shown at the same scale as A, separates uplifted Tahoe moraine to the west from relatively subdued moraine topography across the fault to the east. V.E.—vertical exaggeration.

displacement here is not likely greater than that observed for the eastern splay (~3 m).

The relatively eroded nature of both the Tahoe and pre-Tahoe moraines at Soda Spring prevents accurate estimates of fault displacement on the Kern Canyon fault from these features. Intact portions of the moraine crests do, however, provide some constraints on the total vertical separation across the fault. For the Tahoe moraines, remnants of the western moraine crest are correlated with topographically subdued, partially buried portions of the moraine crest east of the fault (Fig. 2). These portions of the moraine crest are also separated by a relatively intact topographic scarp (Fig. 4C) similar in scale to that observed for the eastern fault strand cutting across the Tioga moraine (Fig. 4A). Isolated remnants of the intact Tahoe crest measured from the lidar DEMs suggest a minimum vertical separation of ~7.5 m across the fault (Fig. 4B). This height difference corresponds to a displacement of at least ~7.8 m for an assumed range of fault dips between 60° and 90°.

Examination of the map pattern of pre-Tahoe moraines suggests that the fault-bounded bedrock ridge effectively split the terminus of the Kern glacier (Fig. 2). As such, an unknown percentage of the total height between moraine remnants on either side of the fault (~40 m) reflects some original elevation difference between these features. This uncertainty precludes conversion of the observed height difference of pre-Tahoe moraine crests to an accurate value of fault displacement.

^{10}Be EXPOSURE DATING AND FAULT SLIP RATES

The late Quaternary slip rate along the Kern Canyon fault was calculated using measurements of cosmogenic ^{10}Be from six granitic boulders on the displaced Tioga moraine. Three large and intact boulders were sampled on each side of the fault to minimize the effects of post-depositional erosion, modification, or burial. Quartz purification and ^{10}Be extraction were completed at Lawrence Livermore National Laboratory (LLNL). Quartz was separated and meteoric ^{10}Be removed using methods described by Kohl and Nishiizumi (1992). The Be carrier used at LLNL is a low-background carrier prepared from beryl with an ~8×10^{-16} ^{10}Be/^{9}Be ratio. After adding Be carrier, quartz was dissolved in an HF/HNO_3 solution. The solution was dried down to remove Si as SiF_6, and fumed several times with $HClO_4$ to evaporate residual fluorides. Be was separated using ion exchange column procedures similar to Stone (2004) with anion exchange using HCl and cation exchange and dilute H_2SO_4 and HCl (Ditchburn and Whitehead, 1994). Be was then precipitated as beryllium hydroxide, ignited to beryllium oxide, mixed with niobium powder, and loaded into stainless-steel cathodes prior to measurement.

Exposure-age calculations were made with the CRONUS-Earth online exposure age calculator, version 2.2, as described in Balco et al. (2008), using a constant production rate model and the scaling scheme for spallation of Lal (1991) and Stone (2000). All model exposure ages assume zero boulder erosion. Table 1 summarizes sample information, ^{10}Be concentrations, and calculated exposure ages. Additional information on the quartz and carrier mass, carrier concentration, and measured isotope ratios is provided in the supplementary materials.[1] The calculated exposure ages form a relatively tight cluster, ranging between 17.4 ± 0.4 and 18.7 ± 0.4 ka. A composite probability distribution function of the six exposure dates reveals an approximately normally distributed spread of ages centered on a mean of 18.1 ± 0.5 ka (Fig. 5A). This composite age is similar to other cosmogenic measurements reported for Tioga moraines elsewhere in the eastern Sierra Nevada (Phillips et al., 2009). Use of a nonconstant production rate for these samples yields a <5% (or <1 k.y.) difference in the calculated exposure ages.

Incorporation of the measured age distribution from the offset Tioga moraine crest into the Monte Carlo simulation yields a normal-sense slip rate for Kern Canyon fault of 0.15 +0.04/–0.02 mm/yr at 95% confidence (Fig. 5B). Rather

[1]GSA Data Repository Item 2010266, Table DR1, additional information on ^{10}Be sample processing and analysis, is available at www.geosociety.org/pubs/ft2010.htm, or on request from editing@geosociety.org, Documents Secretary, GSA, P.O. Box 9140, Boulder, CO 80301-9140, USA.

TABLE 1. ^{10}Be CONCENTRATIONS AND EXPOSURE AGES FOR SODA SPRING MORAINE BOULDERS

Sample name	Latitude (DD) (°N)	Longitude (DD) (°W)	Elevation (m)	Thickness (cm)	Shielding correction*	[^{10}Be] (×10^3 atoms g^{-1})†	Exposure age (ka)§
NF-CRN-01	36.3534	118.4073	2001	4	0.976	307.2 ± 7.4	17.4 ± 0.4
NF-CRN-02	36.3533	118.4073	2001	5	0.976	316.5 ± 5.6	18.1 ± 0.3
NF-CRN-03	36.3532	118.4073	2002	3	0.976	324.9 ± 9.5	18.3 ± 0.5
NF-CRN-04	36.3526	118.4071	1997	4	0.976	329.5 ± 6.2	18.7 ± 0.4
NF-CRN-05	36.3526	118.4069	1999	4	0.976	322.0 ± 6.7	18.3 ± 0.4
NF-CRN-06	36.3527	118.4069	1988	3	0.976	313.4 ± 7.5	17.8 ± 0.4

*Ratio of the production rate at the shielded site to that for a 2π surface at the same location calculated using the CRONUS-Earth Geometric Shielding Calculator, version 2.2.

†Calculated using 07KNSTD ^{10}Be measurement standard and calibration (Nishiizumi et al., 2007).

§Model exposure age assuming no inheritance, zero erosion, density 2.7 g/cm^3 and standard atmosphere calculated with the CRONUS-Earth ^{10}Be–^{26}Al exposure age calculator (Balco et al., 2008), version 2.2, using a constant production rate model and scaling scheme for spallation of Lal (1991) and Stone (2000). This version of the CRONUS calculator uses a reference spallogenic ^{10}Be production rate of 4.49 ± 0.39 atoms g^{-1} yr^{-1} (±1σ, sea-level, high-latitude) and muonogenic production after Heisinger et al. (2002a, 2002b). The quoted uncertainty is the 1σ internal error, which reflects measurement uncertainty only.

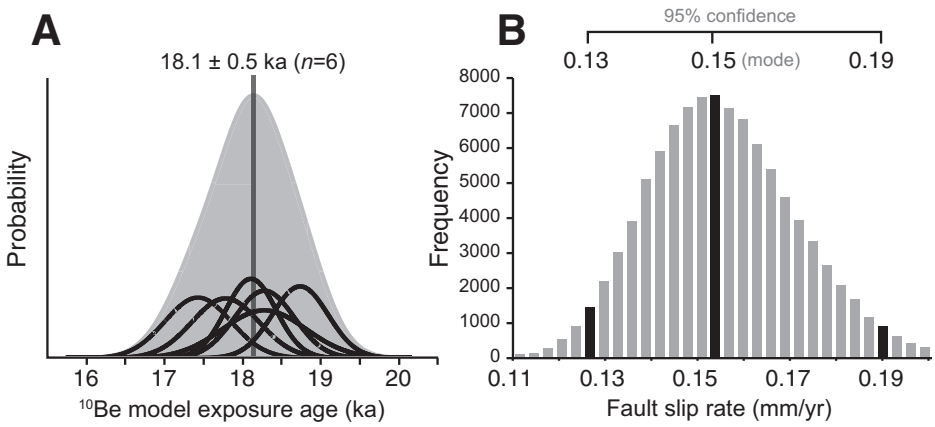

Figure 5. (A) Composite relative probability density function of six exposure ages measured from cosmogenic ^{10}Be on Tioga moraine boulders. The peak age (18.1 ± 0.5 ka) represents a mean of all exposure ages. (B) Histogram of predicted fault slip rates (100,000 trials) for the offset Tioga moraine showing the mode and associated 95% confidence intervals from the Monte Carlo simulation.

than pure uplift or extension, this value represents the most likely rate of fault slip resolved on a planar, steeply east-dipping normal fault dipping anywhere between 60° and 90°. For the Tahoe and pre-Tahoe moraines at Soda Spring, a lack of quantitative age data precludes slip-rate estimates from these features. We do note, however, consistency between the predominately normal offset of these features and the sense of displacement of the Tioga moraine crest.

DISCUSSION

The validity of our estimates of vertical separation, displacement, and fault slip rate for the northern Kern Canyon fault strongly depends on the accuracy of the lidar topography in representing the ground surface at Soda Spring. Although the area immediately surrounding the location of our scarp profile shows only sparse ground cover and few tall trees (Fig. 3A), the bare-earth DEM reflects some degree of smoothing of the raw laser returns in representing the ground surface. This smoothing is evident in the topographic profile along the Tioga moraine crest (Fig. 4A), which shows relatively few variations greater than ~1 m in spite of the presence of large ~2 m boulders on this landform. Nevertheless, the scarp height represented by the topographic profiles corresponds well with our field observations of the prominent, ~4-m-high fault scarp developed on the otherwise continuous Tioga moraine crest (Fig. 3A). Given the comparable ground cover on both sides of the scarp, the degree of smoothing is likely similar along the length of this profile and does not influence the regression slopes used to measure fault displacement and separation.

Fault dip represents the greatest contribution to the uncertainties in our Monte Carlo error simulations. Given the overall linearity of the Kern Canyon fault trace at Soda Spring and elsewhere in Kern Canyon, the fault is either vertical or steeply east-dipping. This observation is confirmed in other locations along the Kern Canyon fault, where detailed field mapping in rugged topography and multiple trench exposures reveal vertical to steeply east-dipping fault planes. Our treatment of fault dip as a uniform distribution from 60° to 90° most likely encompasses the reasonable range in this parameter. Notably, the estimated slip rate of ~0.15 mm/yr at Soda Spring represents a minimum value due to an unknown amount of slip along the secondary western fault strand (Figs. 2 and 3).

Active normal faulting on the Kern Canyon fault is consistent with current patterns of seismogenic deformation in the southern Sierra Nevada. Earthquakes in this region, notably the Durrwood Meadows swarm in the early 1980s (Jones and Dollar, 1986), suggest a localized zone of active horizontal extension and vertical crustal thinning centered over the Kern Plateau (Fig. 1) and high southern Sierra Nevada (Unruh and Hauksson, 2009). Crustal thinning and extension in the southern Sierra Nevada are largely attributed to mantle buoyancy forces related to downwelling lithosphere beneath the adjacent Central Valley (e.g., Ducea and Saleeby, 1996). In this framework, internal deformation of the southern Sierra Nevada is driven by upwelling asthenospheric mantle adjacent to the zone of foundering lithosphere (Saleeby et al., 2009), potentially promoting reactivation of the Kern Canyon fault and normal faulting at Soda Spring.

Rates of normal fault slip on the northern Kern Canyon fault measured at Soda Spring are comparable to Holocene vertical slip rates of ~0.2–0.3 mm/yr measured for the Sierra Nevada frontal fault (Le et al., 2007) bounding Owens Valley to the northeast (Fig. 1). Contemporary vertical deformation values from continuous GPS measurements also suggest on the order of ~0.5 mm/yr of motion for the southern Sierra Nevada (Bennett et al., 2009), although the contribution of postseismic effects from nearby historic earthquakes to this signal remains unclear (Fay et al., 2008). The presence of both the Kern Canyon fault and the Sierra Nevada frontal fault in the area south of latitude ~36.5°N supports an interpretation that the Sierran block may be composed of at least two distinct, west-tilted subblocks (Mahéo et al., 2009; Saleeby et al., 2009). Although comparatively little is known about rates of deformation along the Sierra Nevada frontal fault in the latitude range of the Kern Canyon fault, an abundance of continuous relatively young normal scarps along both the Sierra Nevada frontal fault and the Kern Canyon fault, and comparable slip rates for these two structures (Le et al., 2007) suggest that both

fault systems contribute to active westward tilting of the southern Sierran block.

Recognition of late Quaternary normal faulting on the Kern Canyon fault, and the development of a well-constrained post-Tioga slip rate from this analysis highlight a number of outstanding questions. Importantly, our understanding of the forces driving extensional deformation in the southern Sierra Nevada remains incomplete. The nature of slip-rate variations along the ~140 km length of the Kern Canyon fault is also unknown. Preliminary results of trenching at several sites on the Kern Canyon fault suggest the occurrence of multiple surface-rupturing earthquakes during the Holocene (Kozaci et al., 2009). Whether these ruptures also occurred at Soda Springs is an important element in characterizing local seismic hazards (Kelson et al., 2010) and remains a focus of ongoing research in the area.

CONCLUSION

Measured displacement values and cosmogenic exposure dating of the Tioga moraine crest at Soda Spring provide definitive evidence for late Quaternary activity and the first late Quaternary slip-rate estimate on the northern Kern Canyon fault. This result highlights the utility of lidar topography in identifying and quantifying fault offsets in remote or forested areas and in locations where Quaternary fault offsets have remained cryptic or elusive. The reported normal-sense fault slip rate of ~0.1–0.2 mm/yr suggests that the northern Kern Canyon fault accommodates substantial strain within the Sierra Nevada block, and may play an important role in regional deformation patterns in the southern Sierra Nevada.

ACKNOWLEDGMENTS

This research was supported by the Sacramento District of the U.S. Army Corps of Engineers, as part of the Dam Safety Assurance Program for Isabella Dam, under contract to the URS/Kleinfelder/Geomatrix Joint Venture. Dating analysis was performed under the auspices of the U.S. Department of Energy by Lawrence Livermore National Laboratory under contract DE-AC52-07NA27344. Marco Ticci (William Lettis and Associates, Inc.) provided assistance with geographic information systems (GIS) analysis of the lidar data and digital mapping at Soda Spring. San Joaquin Helicopters of Delano, California, supported our field efforts in northern Kern Canyon. We thank Kurt Frankel for his review comments that substantially improved the manuscript. Hearty thanks go to the Kern Lodge and the Kern River Brewing Company for their hospitality during our stays in Kernville.

REFERENCES CITED

Balco, G., Stone, J., Lifton, N., and Dunai, T., 2008, A complete and easily accessible means of calculating surface exposure ages or erosion rates from ^{10}Be and ^{26}Al measurements: Quaternary Geochronology, v. 3, p. 174–195, doi:10.1016/j.quageo.2007.12.001.

Bennett, R.A., Fay, N.P., Hreinsdottir, S., Chase, C., and Zandt, G., 2009, Increasing long-wavelength relief across the southeastern flank of the Sierra Nevada, California: Earth and Planetary Science Letters, v. 287, p. 255–264, doi:10.1016/j.epsl.2009.08.011.

Busby-Spera, C.J., and Saleeby, J.B., 1990, Intra-arc strike-slip fault exposed at batholithic levels in the southern Sierra Nevada, California: Geology, v. 18, p. 255–259, doi:10.1130/0091-7613(1990)018<0255:IASSFE>2.3.CO;2.

Clark, M.K., Maheo, G., Saleeby, J., and Farley, K.A., 2005, The non-equilibrium landscape of the southern Sierra Nevada, California: GSA Today, v. 15, p. 4–10, doi:10.1130/1052-5173(2005)015[4:TNLOTS]2.0.CO;2.

Dalrymple, G.B., 1963, Potassium-argon dates of some Cenozoic volcanic rocks of the Sierra Nevada, California: Geological Society of America Bulletin, v. 74, p. 379–390, doi:10.1130/0016-7606(1963)74[379:PDOSCV]2.0.CO;2.

Ditchburn, R.G., and Whitehead, N.E., 1994, The separation of ^{10}Be from silicates, *in* Workshop of the South Pacific Environmental Radioactivity Association: South Pacific Environmental Radioactivity Association, p. 4–7.

Ducea, M.N., and Saleeby, J.B., 1996, Buoyancy sources for a large, unrooted mountain range, the Sierra Nevada, California: Evidence from xenolith thermobarometry: Journal of Geophysical Research–Solid Earth, v. 101, p. 8229–8244, doi:10.1029/95JB03452.

Fay, N.P., Bennett, R.A., and Hreinsdottir, S., 2008, Contemporary vertical velocity of the central Basin and Range and uplift of the southern Sierra Nevada: Geophysical Research Letters, v. 35, L20309, doi:10.1029/2008GL034949.

Gillespie, A.R., and Zehfuss, P.H., 2004, Glaciations of the Sierra Nevada, California, USA, *in* Ehlers, J., and Gibbard, P.L., eds., Quaternary Glaciations—Extent and Chronology, Part II: Developments in Quaternary Science, v. 2, part 2, p. 51–62, doi:10.1016/S1571-0866(04)80185-4.

Heisinger, B., Lal, D., Jull, A.J.T., Kubik, P.W., Ivy-Ochs, S., Neumaier, S., Knie, K., Lazarev, V., and Nolte, E., 2002a, Production of selected cosmogenic radionuclides by muons: 1. Fast muons: Earth and Planetary Science Letters, v. 200, p. 345–355, doi:10.1016/S0012-821X(02)00640-4.

Heisinger, B., Lal, D., Jull, A.J.T., Kubik, P.W., Ivy-Ochs, S., Neumaier, S., Knie, K., Lazarev, V., and Nolte, E., 2002b, Production of selected cosmogenic radionuclides by muons: 2. Capture of negative muons: Earth and Planetary Science Letters, v. 200, p. 357–369, doi:10.1016/S0012-821X(02)00641-6.

Jones, L.M., and Dollar, R.S., 1986, Evidence of Basin and Range extensional tectonics in the Sierra Nevada—The Durrwood Meadows swarm, Tulare County, California (1983–1984): Bulletin of the Seismological Society of America, v. 76, p. 439–461.

Kelson, K.I., Simpson, D.T., Rose, R.S., and Serafini, D.C., 2010, Seismic hazard characterization of the Kern Canyon fault for Isabella Dam, California, *in* Proceedings of the 30th Annual Meeting of the United States Society of Dams: Sacramento, California, United States Society of Dams, p. 295–310.

Kohl, C.P., and Nishiizumi, K., 1992, Chemical isolation of quartz for measurement of in-situ–produced cosmogenic nuclides: Geochimica et Cosmochimica Acta, v. 56, p. 3583–3587, doi:10.1016/0016-7037(92)90401-4.

Kozaci, O., Lutz, A., Turner, R., Amos, C., Rose, R., Kelson, K., Baldwin, J., Simpson, D., Maat, P., Kozlowicz, B., Slack, C., Rugg, S., Sowers, J., Brossy, C., Ortiz, R., and Glidden, T., 2009, Evidence for Holocene surface ruptures on the Kern Canyon fault: A former Mesozoic structure of the southern Sierra Nevada, Kern County, California, *in* Seismological Society of America Annual Meeting Abstracts: Seismological Research Letters, v. 80, no. 2, p. 311.

Lal, D., 1991, Cosmic ray labeling of erosion surfaces: In situ nuclide production rates and erosion models: Earth and Planetary Science Letters, v. 104, p. 424–439, doi:10.1016/0012-821X(91)90220-C.

Lawson, A.C., 1904, The Geomorphogeny of the upper Kern Basin: University of California Publications in Geological Sciences Bulletin, v. 3, p. 291–376.

Le, K., Lee, J., Owen, L.A., and Finkel, R., 2007, Late Quaternary slip rates along the Sierra Nevada frontal fault zone, California: Slip partitioning across the western margin of the Eastern California shear zone–Basin and Range Province: Geological Society of America Bulletin, v. 119, p. 240–256, doi:10.1130/B25960.1.

Mahéo, G., Saleeby, J., Saleeby, Z., and Farley, K.A., 2009, Tectonic control on southern Sierra Nevada topography, California: Tectonics, v. 28, TC6006, doi:10.1029/2008TC002340.

Matthes, FE., 1937, The geologic history of Mount Whitney: Sierra Club Bulletin, v. 22, p. 1–18.

Matthes, FE., 1960, Reconnaissance of the Geomorphology and Glacial Geology of the San Joaquin Basin, Sierra Nevada, California: U.S. Geological Survey Professional Paper 329, 62 p.

McCalpin, J.P., 1987, Recommended setback distances from active normal faults, *in* McCalpin, J.P., ed., Proceedings of the 23rd Symposium on Engineering Geology and Soils Engineering: Logan, Utah State University, p. 35–56.

Moore, J.G., and Sisson, T.W., 1984, Geologic map of the Kern Peak quadrangle, Tulare County California: U.S. Geological Survey Geologic Quadrangle Map GQ-1684, scale 1:62,500.

Nadin, E.S., and Saleeby, J.B., 2008, Disruption of regional primary structure of the Sierra Nevada batholith by the Kern Canyon fault system, California, *in* Wright, J.E., and Shervais, J.W., eds., Ophiolites, Arcs, and Batholiths: Geological Society of America Special Paper 438, p. 429–454, doi:10.1130/2008.2438(15).

Nishiizumi, K., Imamura, M., Caffee, M., Southon, J., Finkel, R., and McAnich, J., 2007, Absolute calibration of ^{10}Be AMS standards: Nuclear Instruments & Methods in Physics Research, ser. B, Beam Interactions with Materials and Atoms, v. 258, p. 403–413, doi:10.1016/j.nimb.2007.01.297.

Phillips, F.M., Zreda, M., Plummer, M.A., Elmore, D., and Clark, D.H., 2009, Glacial geology and chronology of Bishop Creek and vicinity, eastern Sierra Nevada, California: Geological Society of America Bulletin, v. 121, p. 1013–1033, doi:10.1130/B26271.1.

Ross, D.C., 1986, Basement-Rock Correlations across the White Wolf–Breckenridge–Southern Kern Canyon Fault Zone, Southern Sierra Nevada, California: U.S. Geological Survey Bulletin 1651, 25 p.

Saleeby, J., Saleeby, Z., Nadin, E., and Maheo, G., 2009, Step-over in the structure controlling the regional west tilt of the Sierra Nevada microplate: Eastern escarpment system to Kern Canyon system: International Geology Review, v. 51, p. 634–669, doi:10.1080/00206810902867773.

Stone, J.O., 2000, Air pressure and cosmogenic isotope production: Journal of Geophysical Research, v. 105, p. 23,753–23,759, doi:10.1029/2000JB900181.

Stone, J.O., 2004, Extraction of Al and Be from quartz for isotopic analysis: University of Washington Cosmogenic Nuclide Laboratory Methods and Procedures, http://depts.washington.edu/cosmolab/chem.html.

Thompson, S.C., Weldon, R.J., Rubin, C.M., Abdrakhmatov, K., Molnar, P., and Berger, G.W., 2002, Late Quaternary slip rates across the central Tien Shan, Kyrgyzstan, central Asia: Journal of Geophysical Research, ser. B, Solid Earth and Planets, v. 107, no. B9, 2203, doi:10.1029/2001JB000596.

Unruh, J., and Hauksson, E., 2009, Seismotectonics of an evolving intracontinental plate boundary, southeastern California, *in* Oldow, J.S., and Cashman, P.H., eds., Late Cenozoic Structure and Evolution of the Great Basin–Sierra Nevada Transition: Geological Society of America Special Paper 447, p. 351–372, doi:10.1130/2009.2447(16).

Webb, R.W., 1946, The geomorphology of the Middle Kern River Basin, southern Sierra Nevada, California: Geological Society of America Bulletin, v. 57, p. 355–382, doi:10.1130/0016-7606(1946)57[355:GOTMKR]2.0.CO;2.

MANUSCRIPT RECEIVED 5 FEBRUARY 2010
REVISED MANUSCRIPT RECEIVED 8 MAY 2010
MANUSCRIPT ACCEPTED 22 JULY 2010

Printed in the USA